JACS
JOURNAL OF THE AMERICAN CHEMICAL SOCIETY
Article
pubs.acs.org/JACS

Photophysical Properties of Self-Assembled Multinuclear Platinum Metallacycles with Different Conformational Geometries

Jun-Sheng Chen,[†,‡] Guang-Jiu Zhao,[†] Timothy R. Cook,[§] Ke-Li Han,*[,†] and Peter J. Stang*[,§]

[†]State Key Laboratory of Molecular Reaction Dynamics, Dalian Institute of Chemical Physics, Chinese Academy of Sciences, Dalian 116023, People's Republic of China

[‡]University of the Chinese Academy of Sciences, Beijing 100049, People's Republic of China

[§]Department of Chemistry, University of Utah, Salt Lake City, Utah 84112, United States

Supporting Information

ABSTRACT: In this work, spectroscopic techniques and quantum chemistry calculations were used to investigate the photophysical properties of various multinuclear platinum complexes with different conformational geometries. This suite of complexes includes a Pt−pyridyl square, a Pt−carboxylate triangle, and a mixed Pt−pyridyl−carboxylate rectangle, as well as two mononuclear Pt model complexes. Studying the individual molecular precursors in the context of larger assemblies is important to provide a complete understanding of the factors governing the observed photophysical properties of a given system. The absorption and emission bands of the parent linear dipyridyl donor (ligand 1) are largely preserved in the [4 + 4] square and the multicomponent [4 + 2 + 2] rectangle (**3** and **4**, respectively), with significant red shifts. The [3 + 3] Pt−carboxylate triangle containing *p*-phthalic acid is nonemissive. Phosphorescence and nanosecond transient spectroscopy on **3** and **4** reveal that the introduction of platinum atoms enhances spin−orbital coupling, thereby increasing the rate of intersystem crossing. This phenomenon is consistent with the low fluorescence quantum yields and short fluorescence lifetimes of **3** and **4**. Moreover, the electronic structures for the ground state and low-lying excited states of these compounds were studied using quantum chemistry calculations. The fluorescent states of the platinum complexes are local excited states of ligand-centered $\pi-\pi^*$ transition features, whereas the nonfluorescent states are intramolecular charge-transfer states. These low-lying intramolecular charge-transfer states are responsible for the nonemissive nature of small molecules **1** and **2** and triangle **5**. As the interactions between these components determine the properties of their corresponding assemblies, we establish novel excited-state decay mechanisms which dictate the observed spectra.

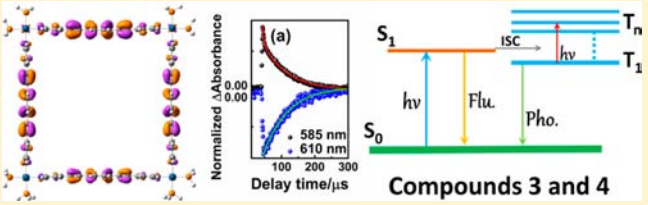

INTRODUCTION

Over the past two decades, coordination-driven self-assembly has provided an effective methodology for constructing novel supramolecular coordination complexes (SCCs) with metal−ligand bonding as the impetus for the formation of single, discrete thermodynamically favored products.[1,2] A variety of organometallic and coordination-based supramolecules with special structures such as one-dimensional (1D) helices, two-dimensional (2D) polygons, and three-dimensional (3D) polyhedra have been reported.[3−5] Palladium, platinum, iridium, and ruthenium ions are important in these supramolecular architectures because they afford stable, predictable coordination spheres to guide directional metal−ligand interactions. These metal nodes complement aromatic compounds such as anthracene, phenanthrene, pyridine, and alkynes, which provide rigid scaffolds to encode directionality in ligands while at the same time imparting interesting photophysical properties to their resulting assemblies. These assemblies are potentially useful for advanced optical and electronic applications owing to the interesting photophysics that arise from the interplay between metal centers and organic ligands.[6−10] As such, the supramolecules formed from the self-assembly of these metals and ligands have been widely investigated in many fields such as synthetic chemistry, medicinal chemistry, biochemistry, bioimaging, photovoltaics, photocatalysis, etc.[3,5,11,12]

Platinum complexes have developed particularly rapidly because of their facile syntheses and varied applications in electroluminescence, photovoltaics, medicinal chemistry, photocatalysis, molecular devices, chemical sensors, nanomaterials, etc.[5,9,13−15] The interest in these complexes has motivated a wide range of studies: Stang et al.[16−19] developed synthetic methodologies to obtain numerous platinum-based SCCs through coordination-driven self-assembly. Particularly relevant to the current study was the discovery that multicomponent assemblies can be quantitatively obtained from systems containing both pyridyl and carboxylate ligands, due to the energetic preference for heteroligated Pt−N,O coordination over homoligated Pt−N,N or Pt−O,O motifs.[17] Goeb et al.[8] synthesized a series of rigid platinum diimine diacetylide complexes with high room temperature (RT) phosphorescence quantum yields and long lifetimes. Zhao et al.[6,9,20,21] developed

Received: March 8, 2013
Published: April 7, 2013

 © 2013 American Chemical Society dx.doi.org/10.1021/ja402421w | J. Am. Chem. Soc. 2013, 135, 6694−6702

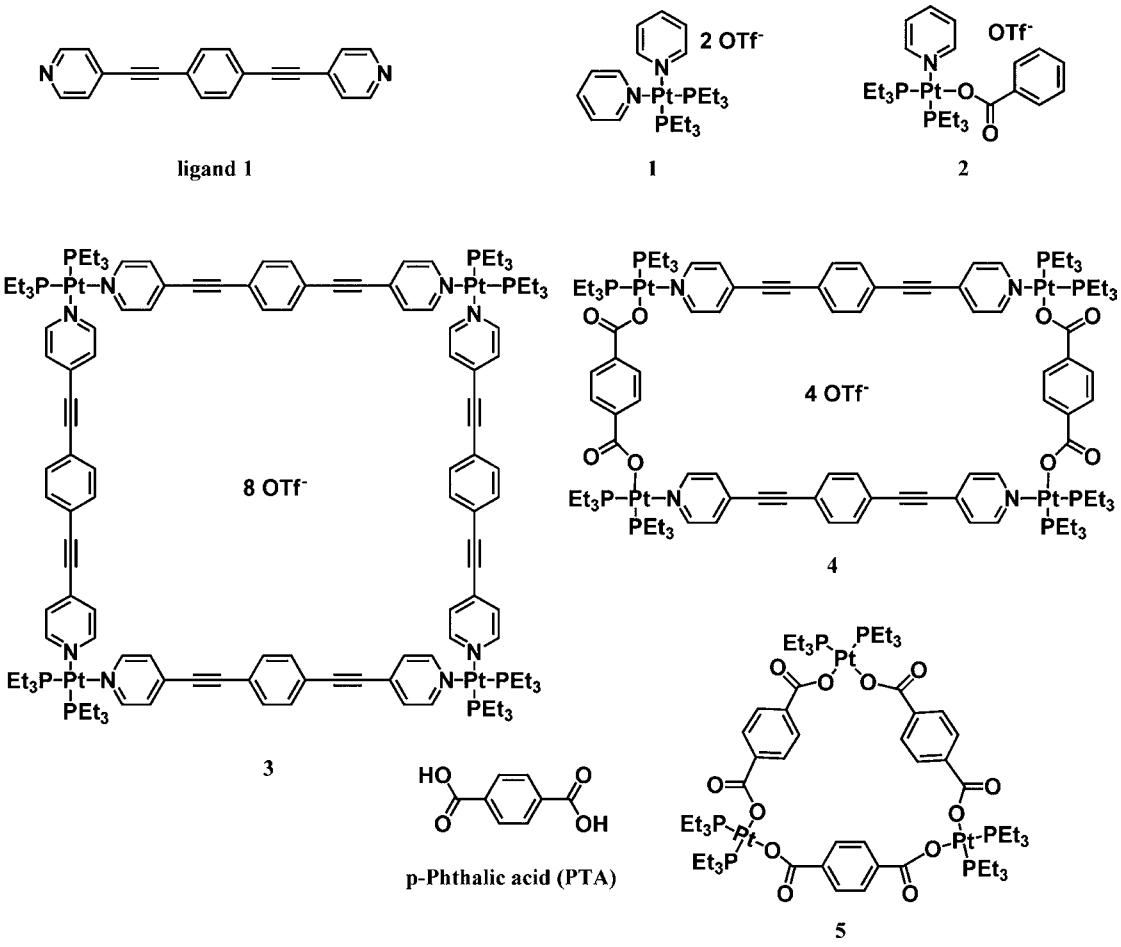

Figure 1. Molecular structures of ligand 1, compounds **1**–**5**, and PTA.

a number of platinum complexes with much longer phosphorescence lifetimes with demonstrative applications in photo-upconversion, oxygen sensing, photoinduced charge transfer, etc. Wong et al.[11,12,22−24] designed a series of new platinum-containing organometallic complexes that exhibit good thermal stability and photophysical properties for solar cell applications. Various experimental techniques and theoretical methods such as two-photon absorption, transient absorption, time-resolved infrared spectroscopy, and density functional theory (DFT)/time-dependent density functional theory (TDDFT) quantum chemistry calculations have been used to study the photophysics and intra/intermolecular energy- and electron-transfer processes of these platinum complexes. Brozik et al.[25] have employed time-resolved infrared spectroscopy to understand platinum acetylide structural changes upon conversion to triplet states. Castellano et al.[15,26,27] performed systematic investigations on the photophysical properties of many platinum complexes using ultrafast transient absorption spectrometry. Goodson et al.[28,29] used femtosecond fluorescence upconversion and transient absorption spectra to investigate platinum-containing SCCs. From these examples, it is clear that the combination of DFT/TDDFT quantum chemistry calculations and experimental spectroscopic methods is an effective way to study the photophysical properties of a number of platinum complexes.[11,16,23,30−35] The inclusion of platinum ions influences the photophysical properties of supramolecules due to spin−orbital coupling, intersystem crossing (ISC) and internal conversion, which affect the lifetime of singlet excited states, phosphorescent quantum yields, etc.[9,36,37] These complexes typically show excited intraligand (IL), metal-to-ligand charge-transfer (MLCT), and ligand-to-metal charge-transfer (LMCT) states, as well as other kinds of intramolecular charge-transfer (ICT) processes.

In the present work we focus specifically on a suite of SCCs formed using a cis-capped 90° Pt acceptor with linear dipyridyl and dicarboxylate donors to determine the effects of conformational geometry and the origins of any electronic transitions and photophysical properties. Spectroscopic and theoretical investigations were employed on seven unique species, including the free ligands, a [4 + 4] square (Pt−N,N coordination, **3**), a multicomponent [4 + 2 + 2] rectangle (Pt−N,O coordination, **4**), a [3 + 3] triangle (Pt−O,O coordination, **5**), [*cis*-Pt$(PEt_3)_2Py_2$](OTf)$_2$ and [*cis*-Pt$(PEt_3)_2$(Py)(Bz)](OTf) (**1** and **2**, respectively; Py = pyridine; Bz = benzoate). A comparison of the steady-state absorption and fluorescence spectra and fluorescence lifetimes of these supramolecules and their ligands affords insight into the ramifications of incorporating Pt into an SCC scaffold. Furthermore, the phosphorescence emission and nanosecond transient absorption spectra of **4** and **5** were obtained and discussed along with relevant DFT and TDDFT results, providing information about the nature of the low-lying excited states in these complexes.

dx.doi.org/10.1021/ja402421w | J. Am. Chem. Soc. 2013, 135, 6694−6702

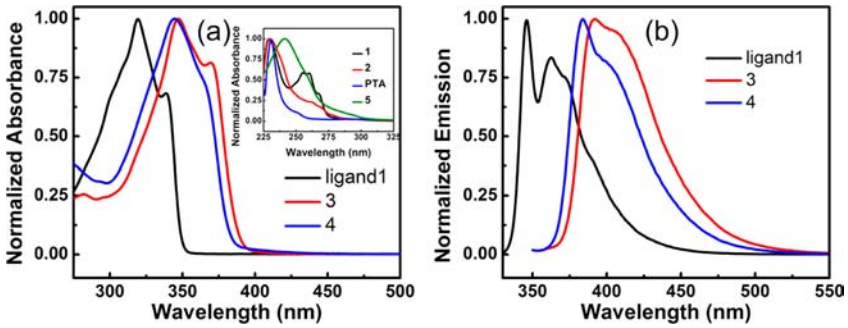

Figure 2. Normalized steady-state absorbance and emission spectra of ligand 1, PTA, and **1**–**5**. (a) Absorbance spectra of ligand 1, **3**, and **4**. Inset: spectra of **1**, **2**, **5**, and PTA. (b) Fluorescence emission spectra of ligand 1 (λ_{ex} = 320 nm), square **3** (λ_{ex} = 347 nm), and rectangle **4** (λ_{ex} = 343 nm).

EXPERIMENTAL AND THEORETICAL METHODS

The homoligated molecule [*cis*-Pt(PEt_3)$_2$$Py_2$](OTf)$_2$ (**1**), heteroligated [*cis*-Pt(PEt_3)$_2$(Py)(Bz)](OTf) (**2**),[17] square **3**, rectangle **4**, triangle **5**, and 1,4-bis(4-pyridylethynyl)benzene (ligand 1)[17,38] were prepared according to literature procedures (see Figure 1). *p*-Phthalic acid (PTA) was purchased from Aladdin Chemistry Co. Ltd. and used without further purification. Unless otherwise stated, all absorption and emission experiments were conducted in dichloromethane (DCM, CH_2Cl_2). All solvents used were high-performance liquid chromatography grade.

UV–vis absorption spectra were obtained using an HP 8453 spectrophotometer. The steady-state fluorescence, phosphorescence, and time-resolved fluorescence decays were recorded using a Horiba Jobin Yvon FluoroMax-4 spectrofluorometer. Time-resolved fluorescence decays were recorded using the time-correlated single photon counting method. Data analysis was conducted using commercial software provided by Horiba Instruments. Nanosecond transient absorption experiments were carried out using a pump–probe setup. All samples were thoroughly degassed prior to obtaining steady-state phosphorescence and nanosecond transient absorption spectra.

Ground-state geometry optimizations were carried out using the TURBOMOLE program suite by DFT with the BP86 functional and RI approximation,[39−46] which is widely used in large-molecule systems.[31−35] To obtain a good description of the electron correlation in the excitation processes, the TDDFT method with the cam-B3LYP functional was adopted to investigate the excited states of these supramolecules.[12,47,48] All excited-state calculations were performed using Gaussian 09,[49] and solvent effects were included using the integral equation formalism (IEF) version of the polarizable continuum model (PCM) with the dielectric constant of dichloromethane (ε = 8.93). Throughout the ground-state optimizations and excited-state studies, the SVP basis set was chosen for nonmetallic elements and the def-TZVP and pseudopotential def-ecp basis sets were selected for platinum atoms.[41,50]

RESULTS AND DISCUSSION

Steady-State Absorption and Emission. The steady-state absorption spectra of ligand 1, PTA and compounds **1**–**5** are shown in Figure 2a, and the fluorescence emission spectra of ligand 1, **3**, and **4** are shown in Figure 2b. The absorption, fluorescence emission, and fluorescence quantum yields are listed in Table 1. Although the band shapes of the spectra of **3**–**5** are similar to those of their corresponding ligands (PTA or ligand 1), the absorption bands of the SCCs are notably red-shifted. The main absorption band of **5** (λ_{max} = 241 nm) is red-shifted by 10 nm compared to that of PTA (λ_{max} = 231 nm). The shifts associated with ligand 1 and its corresponding SCCs are even greater, with the dominant absorption bands of **3** and **4** appearing red-shifted by ∼25 nm. The absorption spectrum of ligand 1 has a main peak (319 nm) and a shoulder peak (339 nm), with **3** and **4** showing similar vibronic progressions, albeit clearer for **3** than for **4**. Compound **3** is slightly more red-shifted (∼2 nm) than **4**, which is ascribed to the presence of PTA at the expense of two more molecules of ligand 1 in the latter. The mononuclear Pt compounds **1** and **2** are models of the metal nodes in **3** and **4**. Their absorption bands (inset of Figure 2a) are centered about 230 nm. Given the significantly better match between the spectrum of ligand 1 and the features observed in the spectra of **3**–**5** over those of the spectra of **1** and **2**, the transitions present in the SCCs are likely ligand-centered and undergo shifts due to the presence of Pt.

Table 1. Summary of Steady-State Absorption, Emission, and Fluorescence Quantum Yield (Φ) Measurements

compd	absorption band λ_{max}/nm [$\varepsilon \times 10^4$/cm^{-1}·M^{-1}]	λ_{ex} /nm	λ_{em} /nm	Φ
ligand 1	319 [4.8], 339 [3.3]	320	346, 363	0.395 ± 0.002
1	229 [1.9], 255 [0.7], 260 [0.7], 267 [0.4]			
2	230 [1.5], 260 [0.4]			
3	347 [25.4], 367 [20.9]	347	392, 408	0.167 ± 0.001
4	345 [9.3], 365 [6.8]	343	384, 400	0.124 ± 0.003
5	241 [4.7]			
PTA	231 [1.7], 250 [0.2]			

No fluorescence emission was observed for compounds **1**, **2**, and **5**. The fluorescence emission spectra of ligand 1, **3**, and **4** are shown in Figure 2b, again with red shifts observed between the SCCs and the dipyridyl ligand. The band shapes of all three compounds are all similar, with a double-peak structure that parallels the absorption spectra. Thus, the fluorescence emission states are dominated by ligand-centered features. The Stokes shift of ligand 1 is 27 nm, increasing to 45 and 39 nm for **3** and **4**, respectively. The increased shifts associated with the SCCs suggest that their fluorescence states may possess ICT character and indicate that Pt directly influences the fluorescence states. In addition, the larger Stokes shift of **3** versus that of **4** further indicates that the ligands present also play a role in determining not only the band shape, but also the λ_{em} of a given SCC. The fluorescence quantum yields (Table 1) of ligand 1, **3**, and **4** are 39.5%, 16.7%, and 12.4%, respectively, collected relative to anthracene (Φ_F = 27% in ethanol).[51] The attenuated quantum yields of the SCCs versus the free dipyridyl ligand are ascribed to spin–orbit coupling that occurs upon the inclusion of the heavy Pt centers. This spin–orbit coupling increases the rate of ISC, inducing the fluorescence quenching. Furthermore, the quantum yield of **4** is smaller than that of **3**. As with the absorption spectra of this suite of compounds, the

dx.doi.org/10.1021/ja402421w | J. Am. Chem. Soc. 2013, 135, 6694−6702

presence of Pt has a marked effect on the emission spectra of **3** and **4**, manifesting energy shifts in fluorescence as well as affecting quantum yields from excited states that appear to be largely ligand-centered.

Time-Resolved Fluorescence Spectra. To further understand the role of Pt on the fluorescent excited states of **3** and **4**, the time-resolved fluorescence decays of ligand 1, **3**, and **4** (λ_{ex} = 295 or 376 nm) were measured, monitored at the maximum λ_{em} for each compound. Figure 3 shows the kinetic traces used

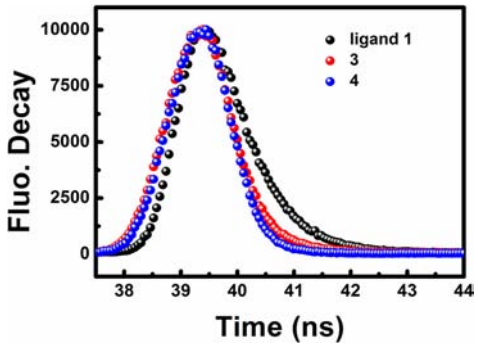

Figure 3. Time-resolved fluorescence decays of ligand 1 (λ_{ex} = 295 nm), **3**, and **4** (λ_{ex} = 376 nm) monitored at the peak emission wavelength for each species. The "rise" feature is due to the pulsed nano-LED source (laser). The instrument response functions (IRFs) are displayed in Supporting Information Figure S1. The fluorescence lifetimes were obtained by convoluting the singles with the IRFs.

to determine the fluorescent excited-state lifetimes, which are summarized in Table 2. The monoexponential lifetime values of

Table 2. Summary of Lifetime Measurements of the Fluorescent Excited State of ligand 1, 3, and 4 Using Monoexponential Decays[a]

compd	λ_{ex} /nm	λ_{em} /nm	τ/ns	χ^2
ligand 1	295	345	0.5239 ± 0.0026	1.3477
3	376	393	0.3736 ± 0.0013	1.1587
4	376	398	0.1717 ± 0.0034	1.1944

[a]The quality of the single-exponential fit was measured by the χ^2 values.

ligand 1, **3**, and **4** are 0.52, 0.37, and 0.17 ns, respectively. The significantly lower values for the SCCs are consistent with a Pt-enhanced ISC rate or enhanced ICT due to the presence of the heavy metal ions. Compound **4** has a noticeably shorter lifetime than **3**, indicating that the specific ligands used can also affect the emissive process of metallacycles.

Phosphorescence Emission Spectra. The phosphorescence emission spectra of **3** and **4** were measured at RT and at 77 K in degassed dichloromethane (Figure 4), with the data summarized in Table 3. At RT, peak maxima were observed at 392 and 384 nm for **3** and **4**, respectively, which correspond to the fluorescence emission peaks discussed previously. In addition, a small peak at 542 nm and a shoulder peak at 580 nm were observed for both compounds. Cooling to 77 K helps resolve these features, manifesting in an increase of the emission intensity of the low-energy bands while simultaneously attenuating the fluorescence intensity. These spectral changes indicate that the emission centered about 400 nm is due to delayed fluorescence, whose intensity is decreased with decreased temperature.[52] The low-energy emission peaks are

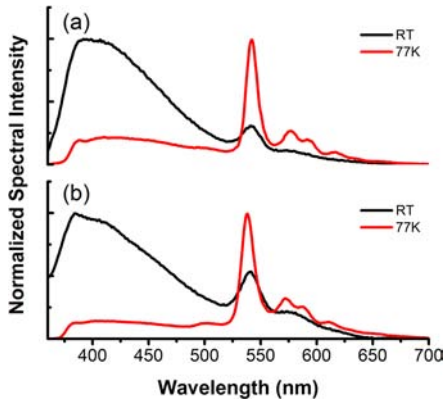

Figure 4. Normalized steady-state phosphorescence emission spectra at room temperature (black) and 77 K (red, λ_{ex} = 344 nm) for (a) compound **3** and (b) compound **4**.

phosphorescence emission. The lifetime values measured using the delayed fluorescence bands for **3** and **4** are 18.3 and 18.4 μs, respectively.

The triplet excited-state emission was most apparent when measured at 77 K, revealing a dominant phosphorescent peak at 541 nm and three small peaks at 577, 592, and 616 nm for **3**. Compound **4** showed similar features, with minor blue shifts relative to their counterparts in **3**, with a maximum at 538 nm and three small peaks at 572, 586, and 611 nm. The thermally induced Stokes shift ($\Delta E_s = E_{00}(77\ K) - E_{00}(RT)$) is an indication of an ^{3}IL or ^{3}MLCT feature of an emissive triplet excited state.[53] Here, the thermally induced Stokes shifts in **3** (ΔE_s = 34 cm^{-1}) and **4** (ΔE_s = 137 cm^{-1}) are small, demonstrating that ^{3}IL is the major component of the emissive triplet excited states.[8,9]

Nanosecond Transient Absorption Spectra. The nanosecond transient absorption spectra of **3** and **4** (λ_{ex} = 355 nm) were measured, monitored at different wavelengths. Three characteristic dynamic processes were observed: (i) triplet excited-state absorption (ESA), (ii) triplet excited-state stimulated emission (SE), and (iii) ground-state bleaching (GSB). Figure 5 shows the triplet ESA and triplet SE signals monitored at 585 and 610 nm, respectively, with fitted results summarized in Table 4. For compounds **3** and **4**, the triplet SE and ESA processes could be fit by mono- and biexponential behaviors. The triplet SE signal corresponds to the triplet excited-state emission process, with the monoexponential lifetime indicative of phosphorescence. The phosphorescence emission lifetime values of **3** and **4** are 64 and 77 μs, respectively. The combination of the aforementioned small thermally induced Stokes shifts and an emission lifetime leaves little doubt that the triplet excited-state decays of compounds **3** and **4** are dominated by ^{3}IL states.[21,53] The triplet ESA processes were fit to biexponential functions. The longer lifetime components of these fits (τ_2) are 64 (for **3**) and 79 μs (for **4**), in accordance with the phosphorescence emission lifetime values. The shorter lifetime values (τ_1) are 4.7 μs for both species. Since the delayed fluorescence emission processes exhibited relatively longer lifetimes (~18 μs) for both **3** and **4**, the fast decay component of the triplet ESA process may be ascribed to a reverse intersystem crossing (RISC) process, wherein these compounds transition back from their triplet excited states to singlet excited states. The GSB signals were fit with biexponential functions, as shown in Figure 6. These fits

dx.doi.org/10.1021/ja402421w | J. Am. Chem. Soc. 2013, 135, 6694−6702

Table 3. Summary of Delayed Fluorescence and Phosphorescence Emission of 3 and 4

compd	$\lambda_{\text{delayed fluo}}$(RT)/nm	λ_{phos}(RT)/nm	λ_{phos}(77 K)/nm	ΔE_s/cm^{-1}	$\tau_{\text{delayed fluo}}$(RT)/$\mu$s	τ_{phos}(RT)/μs	τ_{phos}(77 K)/ms
3	392	542, 580	541, 577, 592, 616	34	18.3 ± 0.3	64 ± 1	5.54 ± 0.01
4	384	542, 580	538, 572, 586, 611	137	18.4 ± 0.3	77 ± 4	7.95 ± 0.08

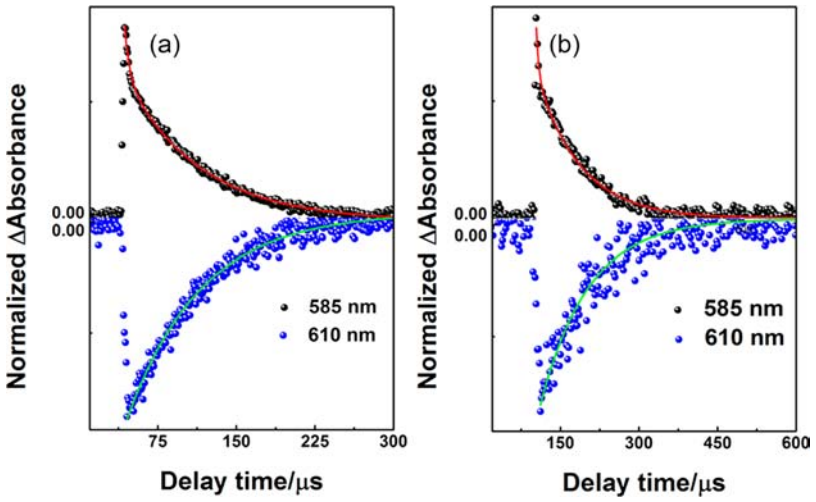

Figure 5. Normalized nanosecond transient absorption spectra of **3** (a) and **4** (b) in DCM (λ_{ex} = 355 nm) monitored at 585 and 610 nm.

Table 4. Summary of Transient Kinetic Time Constants for 3 and 4

	λ_{probe} = 360 nm		λ_{probe} = 585 nm		λ_{probe} = 610 nm
compd	τ_1/μs	τ_2/μs	τ_1/μs	τ_2/μs	τ/μs
3	2.9 ± 0.1	69 ± 1	4.7 ± 1	64 ± 1	64 ± 1
4	3.4 ± 0.1	88 ± 1	4.7 ± 1	79 ± 1	77 ± 4

produced lifetime values of 2.9 and 69 μs for **3** and 3.4 and 88 μs for **4**.

DFT and TDDFT Calculations. The ground-state optimized structures of compounds **1**−**5** are shown in Figure 7, with relevant bond distances, bond angles, and dihedral angles summarized in Table S1 (Supporting Information). The calculated platinum−nitrogen bond distance of approximately 2.1 Å, platinum−phosphorus bond distance of approximately 2.3 Å, and nitrogen−platinum−nitrogen and phosphorus−platinum−phosphorus bond angles are close to typical experimental values. For compounds **3** and **4**, the calculated bond angles of the square coordination environment about platinum range from 82.9° to 88.8°, approaching the idealized 90°. The calculated nitrogen−platinum−nitrogen bond angles in compound **3** are much closer to 90° than in compound **4**, indicating that Pt−N and Pt−O configurations cause alternative angularities. The dihedral angles Pt_1−Pt_2−Pt_3−Pt_4 of compounds **3** and **4** and O_1−Pt_1−Pt_2−Pt_3 of compound **5** are 0.011°, 0.068°, and 0.086°, respectively, which are close to the value expected for untwisted structures (0°). Thus, the platinum ions are coplanar, demonstrating that the optimized structures of compounds **3**−**5** are consistent with the designation of square, rectangle and triangle metallacyclic configurations, respectively.

The calculated electronic transition energies and corresponding oscillator strengths (f) of the low-lying excited states for compounds **1**−**5** are listed in Table 5 and Tables S2−S6 (Supporting Information), which show that the calculated longest wavelength absorptions for compounds **1**−**5** are at 228, 230, 372, 364, and 239 nm, respectively, consistent with the experimental results discussed previously. The corresponding oscillator strengths (f) of the low-lying singlet excited states for compounds **1**, **2**, and **5** approach zero. These states also exhibit charge-transfer character, including MLCT, LMCT, ILCT, ligand-to-ligand charge transfer (LLCT), and metal-to-metal charge transfer. These charge-transfer excited states with corresponding oscillator strengths approaching zero may lead to the fluorescence quenching of these compounds. By

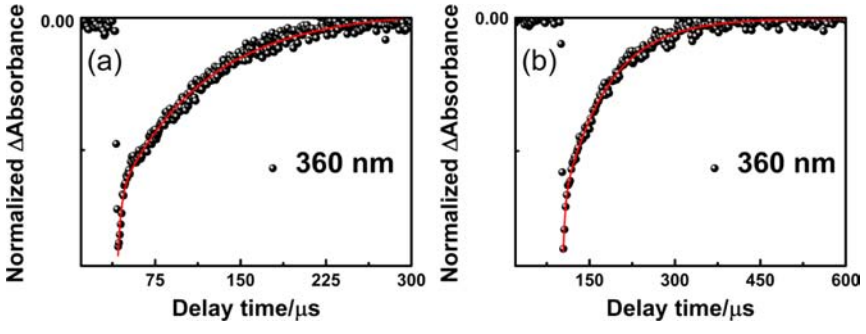

Figure 6. Normalized nanosecond transient absorption spectra of **3** (a) and **4** (b) in DCM (λ_{ex} = 355 nm) monitored at 360 nm.

dx.doi.org/10.1021/ja402421w | J. Am. Chem. Soc. 2013, 135, 6694−6702

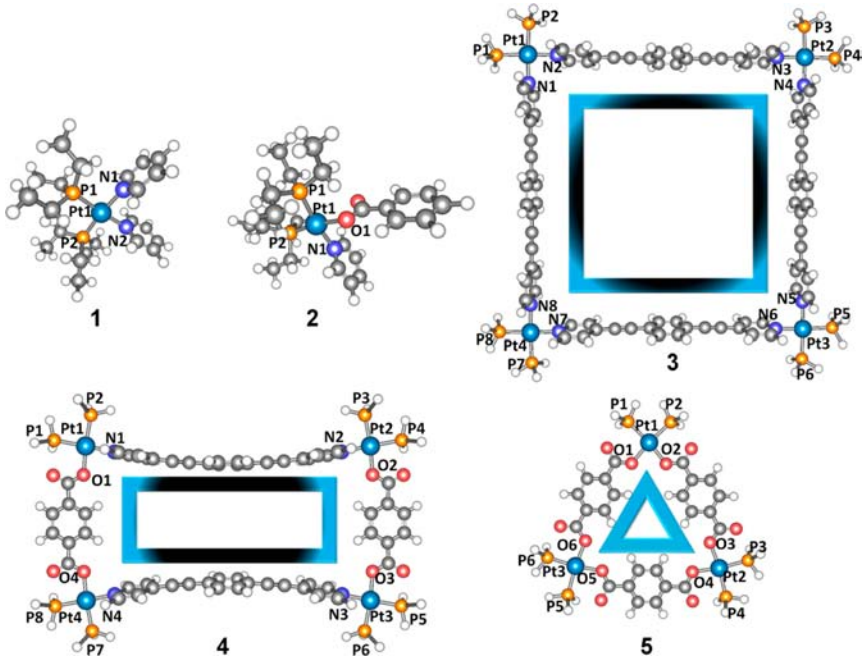

Figure 7. Views of the optimized structures of **1**−**5**: gray, C; blue, N; red, O; white, H; cyan, Pt; orange, P.

Table 5. Selected Calculated Electronic Transition Energies and Corresponding Oscillator Strengths of the Low-Lying Singlet Excited States of Compounds 1−5[a]

compd	electronic transition	absorption wavelength/nm (energy/eV)	f	contrib	CI	character
1	$S_0 \rightarrow S_7$	228 (5.43)	0.0659	H − 2 → L	0.267	MLCT, IL
				H − 1 → L + 1	0.318	IL
2	$S_0 \rightarrow S_8$	230 (5.39)	0.0331	H − 6 → L	0.391	MLCT, IL
3	$S_0 \rightarrow S_2$	372 (3.33)	5.1956	H − 3 → L + 2	0.121	IL
				H − 1 → L	0.220	IL, LLCT
				H − 1 → L + 3	0.214	IL, LLCT
				H → L + 1	0.145	IL
	$S_0 \rightarrow S_3$	372 (3.33)	5.1983	H − 3 → L + 1	0.129	IL
				H − 2 → L	0.219	IL, LLCT
				H − 2 → L + 3	0.204	IL, LLCT
				H → L + 2	0.145	IL
4	$S_0 \rightarrow S_2$	364 (3.41)	5.1634	H − 1 → L	0.446	IL, LLCT
				H → L + 1	0.447	IL, LLCT
5	$S_0 \rightarrow S_{23}$	239 (5.19)	1.6592	H − 2 → L	0.310	IL, LLCT
				H → L + 3	0.238	IL, LLCT
	$S_0 \rightarrow S_{24}$	239 (5.19)	1.6524	H − 1 → L	0.303	IL
				H → L + 4	0.277	IL

[a]H means highest occupied molecular orbital (HOMO), and L means lowest unoccupied molecular orbital (LUMO). IL = intraligand, MLCT = metal-to-ligand charge transfer, and LLCT = ligand-to-ligand charge transfer.

contrast, the bright excited states of compounds **1**−**5** mainly exhibit IL features, as listed in Table 5, with some contributions from ICT. The contribution from ICT likely induces the red shift of the absorption bands of compounds **1**− **5** relative to the free ligands.

As shown in Table 5, the bright state (S_7) of **1** corresponds to the orbital transition of the HOMO − 2 to the LUMO or the HOMO − 1 to the LUMO + 1. The bright state (S_8) of **2** corresponds to the orbital transition from the HOMO − 6 to the LUMO. Bright states S_{23} and S_{24} of compound **5** correspond to the contribution of the HOMO − 2 to the LUMO, the HOMO to the LUMO + 3, the HOMO − 1 to the LUMO, and the HOMO to the LUMO + 4. For **3**, the excited states S_1, S_2, S_3, and S_4 are degenerate. The frontier molecular orbitals comprising the HOMO − 3 to the LUMO + 3 contribute to these excited-state transitions. For compound **4**, the excited states S_1 and S_2 are degenerate states and frontier molecular orbitals spanning the HOMO − 1 to the LUMO + 1 are involved in these transitions. Figure 8 shows that the calculated frontier molecular orbitals for these low-lying, bright excited-state transitions of compounds **1**−**5** possess the same features. The electron densities of the orbitals with π-type symmetry are significantly localized on the ligands of each compound; i.e., the bright states of these compounds may be regarded as $\pi \rightarrow \pi^*$ transitions. The first allowed transitions for **1** are the HOMO − 2 → LUMO and the HOMO − 1 → LUMO + 1 ($f \approx 0.07$), and these transitions extend to the platinum ions. For compound **2**, the first allowed transition is

dx.doi.org/10.1021/ja402421w | J. Am. Chem. Soc. 2013, 135, 6694−6702

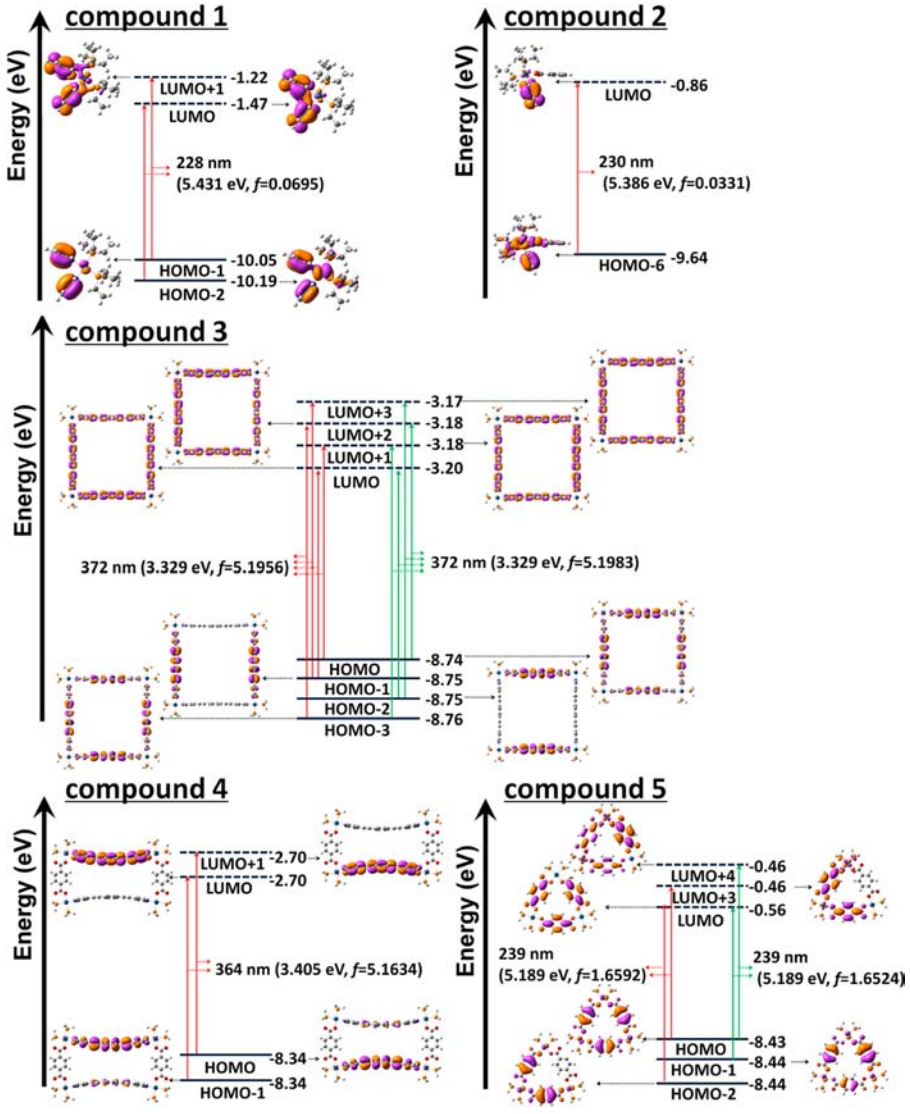

Figure 8. Calculated frontier molecular orbitals for the low-lying bright states of compounds **1**−**5**.

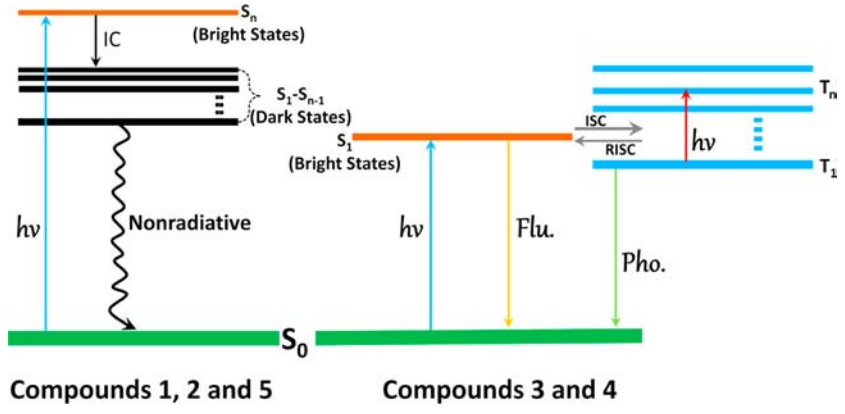

Figure 9. Mechanism of the various excited-state decay pathways for **1**−**5**.

the HOMO − 6 → LUMO ($f \approx 0.03$) predominantly described as an IL feature with some contribution from an MLCT. For compound **3**, absorption primarily occurs from several degenerate states with mixed HOMO − 3 → LUMO + 2, HOMO − 1 → LUMO, HOMO − 1 → LUMO + 3, HOMO → LUMO + 1, HOMO − 3 → LUMO + 1, HOMO − 2 → LUMO, HOMO − 2 → LUMO + 3, and HOMO → LUMO + 2 in the transitions ($f \approx 5.20$), which are characterized as an admixture of IL and LLCT. Compound **4** also exhibits low-energy transitions, HOMO − 1 → LUMO and HOMO → LUMO + 1 ($f \approx 5.16$), with a mix of IL and LLCT features. The important transition of compound **5**

dx.doi.org/10.1021/ja402421w | J. Am. Chem. Soc. 2013, 135, 6694−6702

comprises two degenerate states with a mixture of HOMO − 2 → LUMO, HOMO → LUMO + 3, HOMO − 1 → LUMO, and HOMO → LUMO + 4 (f∼1.65), which possess IL and LLCT characters.

The different kinetic schemes for compounds **1**−**5** in the low-lying excited states are shown in Figure 9. Compounds **1**, **2**, and **5** can be photoexcited to a bright state (S_n) located above several dark or forbidden transition states (S_{n-1}−S_1). These compounds can decay to a dark state by internal conversion, after which they can decay to the ground state through a nonradiative transition pathway. These nonradiative transition processes induce fluorescence quenching. In contrast, compounds **3** and **4** can be directly excited to a bright state, a radiative state occupying the lowest energy level. Once in these bright excited states, these SCCs decay to the ground state through different pathways. Direct relaxation from the low-lying bright state to the ground state is detected as fluorescence. On the other hand, the low-lying singlet excited states for compounds **3** and **4** may also populate low-lying triplet states, particularly facilitated by the presence of Pt ions which enhance ISC effects. The molecules that undergo ISC to transition from the singlet to low-lying triplet states may undergo RISC to repopulate the singlet state, which gives rise to delayed fluorescence. Alternatively, these complexes may directly relax from their triplet excited states via a radiative process, giving rise to the observed phosphorescence emission. The different excited-state kinetic processes of these SCCs and model complexes indicate that specific interactions between the metal nodes and ligands present play an important role in the electronic transitions and observed photophysical properties.

CONCLUSION

We investigated the photophysical properties of platinum-containing SCCs using time-resolved spectroscopic experiments and quantum chemistry calculations. The introduction of platinum atoms resulted in a red shift of both the absorption and emission spectra relative to those of the free ligands. For compounds **1**, **2** and **5**, no fluorescence emission was observed. The fluorescence quantum yields for the square (**3**) and rectangle (**4**) metallacycles were lower than that of the dipyridyl ligand, consistent with significantly reduced fluorescence lifetimes. The combination of small thermally induced Stokes shifts in the phosphorescence emission spectra and long phosphorescence emission lifetimes in the nanosecond transient spectra demonstrated that ^{3}IL was the major component of the emissive triplet excited states of compounds **3** and **4**. Furthermore, we calculated the electronic structures for the ground and low-lying excited states of compounds **1**−**5** using DFT/TDDFT methods. The optimized structures of compounds **3**−**5** were consistent with the expected square, rectangle, and triangle metallacyclic configurations. In addition, the low-lying excited-state transition computational results indicated that these platinum complexes possess different excited-state decay processes, which explains the different steady-state emission observed experimentally. Compounds **1**, **2**, and **5** can be photoexcited to bright states (S_n) which are located above several dark states (S_{n-1}−S_1). These ^{1}IL states decay to dark states by nonradiative processes which then further relax to the ground state through additional nonradiative transitions. In contrast, compounds **3** and **4** can be directly excited to the ^{1}IL bright state, a radiative state that decays back to the ground state and gives rise to the observed fluorescence of these two SCCs. Alternatively, the ^{1}IL excited states may undergo ISC to ^{3}IL excited states which possess long lifetimes and give rise to phosphorescence and RISC to give delayed fluorescence. The presence of platinum ions greatly influenced the electronic states of these complexes. For compounds **1**, **2**, and **5**, the introduction of platinum atoms induced multiple ICT dark states under the bright states, which led to complete fluorescence quenching. In compounds **3** and **4**, the introduction of platinum ions enhanced the spin−orbital coupling, ultimately increasing the rate of intersystem crossing. This phenomenon resulted in the low fluorescence quantum yield and reduced fluorescence lifetimes of compounds **3** and **4** relative to ligand 1. These results indicate that a careful consideration of both the metal nodes and ligands used is necessary to control the photophysical properties of SCCs, particularly given the various conformational geometries which result from the combination of different ligands to afford architectures with desired functionalities.

ASSOCIATED CONTENT

Supporting Information

Instrument response functions, calculated bond lengths, angles, and dihedral angles of the optimized structures of **1**−**5**, and calculated electronic transition energies and corresponding oscillator strengths of the low-lying singlet excited states of **1**−**5**. This material is available free of charge via the Internet at http://pubs.acs.org.

AUTHOR INFORMATION

Corresponding Author

klhan@dicp.ac.cn; Stang@chem.utah.edu

Notes

The authors declare no competing financial interest.

ACKNOWLEDGMENTS

This work was supported by the National Natural Science Foundation of China (NSFC; Grant 21273234) and National Key Basic Research Science Foundation of China (NKBRSF; Grant 2013CB834604). P.J.S. thanks the National Science Foundation (NSF; Grant 1212799) for financial support. G.J.Z. thanks the Frontier Science Project of the Knowledge Innovation Program of the Chinese Academy of Sciences (CAS) for financial support.

REFERENCES

(1) Cook, T. R.; Zheng, Y. R.; Stang, P. J. *Chem. Rev.* **2013**, *113*, 734.
(2) Seidel, S. R.; Stang, P. J. *Acc. Chem. Res.* **2002**, *35*, 972.
(3) Chakrabarty, R.; Mukherjee, P. S.; Stang, P. J. *Chem. Rev.* **2011**, *111*, 6810.
(4) Stang, P. J.; Olenyuk, B. *Acc. Chem. Res.* **1997**, *30*, 502.
(5) Amouri, H.; Desmarets, C.; Moussa, J. *Chem. Rev.* **2012**, *112*, 2015.
(6) Ji, S. M.; Wu, W. H.; Wu, W. T.; Guo, H. M.; Zhao, J. Z. *Angew. Chem., Int. Ed.* **2011**, *50*, 1626.
(7) Yam, V. W. W. *Acc. Chem. Res.* **2002**, *35*, 555.
(8) Goeb, S.; Prusakova, V.; Wang, X.; Vezinat, A.; Salle, M.; Castellano, F. N. *Chem. Commun.* **2011**, *47*, 4397.
(9) Wu, W.; Sun, J.; Ji, S.; Wu, W.; Zhao, J.; Guo, H. *Dalton Trans.* **2011**, *40*, 11550.
(10) Zhao, X. H.; Xie, G. H.; Liu, Z. D.; Li, W. J.; Yi, M. D.; Xie, L. H.; Hu, C. P.; Zhu, R.; Zhao, Q.; Zhao, Y.; Zhao, J. F.; Qian, Y.; Huang, W. *Chem. Commun.* **2012**, *48*, 3854.
(11) Zhou, G. J.; Wong, W. Y. *Chem. Soc. Rev.* **2011**, *40*, 2541.
(12) Wong, W. Y.; Ho, C. L. *Coord. Chem. Rev.* **2006**, *250*, 2627.

(13) Shanmugaraju, S.; Vajpayee, V.; Lee, S.; Chi, K. W.; Stang, P. J.; Mukherjee, P. S. *Inorg. Chem.* **2012**, *51*, 4817.
(14) Du, P.; Schneider, J.; Fan, L.; Zhao, W.; Patel, U.; Castellano, F. N.; Eisenberg, R. *J. Am. Chem. Soc.* **2008**, *130*, 5056.
(15) Muro, M. L.; Rachford, A. A.; Wang, X.; Castellano, F. N. Platinum(II) Acetylide Photophysics. In *Photophysics of Organometallics*; Lees, A. J., Ed.; Springer-Verlag: Berlin, 2010; Vol. *29*, pp 159−191.
(16) Pollock, J. B.; Cook, T. R.; Stang, P. J. *J. Am. Chem. Soc.* **2012**, *134*, 10607.
(17) Zheng, Y. R.; Zhao, Z. G.; Wang, M.; Ghosh, K.; Pollock, J. B.; Cook, T. R.; Stang, P. J. *J. Am. Chem. Soc.* **2010**, *132*, 16873.
(18) Zheng, Y. R.; Lan, W. J.; Wang, M.; Cook, T. R.; Stang, P. J. *J. Am. Chem. Soc.* **2011**, *133*, 17045.
(19) Zheng, Y. R.; Stang, P. J. *J. Am. Chem. Soc.* **2009**, *131*, 3487.
(20) Zhao, J. Z.; Ji, S. M.; Wu, W. H.; Wu, W. T.; Guo, H. M.; Sun, J. F.; Sun, H. Y.; Liu, Y. F.; Li, Q. T.; Huang, L. *RSC Adv.* **2012**, *2*, 1712.
(21) Ji, S. M.; Wu, W. H.; Wu, W. T.; Song, P.; Han, K. L.; Wang, Z. G.; Liu, S. S.; Guo, H. M.; Zhao, J. Z. *J Mater. Chem.* **2010**, *20*, 1953.
(22) Wang, Q. W.; Wong, W. Y. *Polym. Chem.* **2011**, *2*, 432.
(23) Dai, F. R.; Zhan, H. M.; Liu, Q.; Fu, Y. Y.; Li, J. H.; Wang, Q. W.; Xie, Z. Y.; Wang, L. X.; Yan, F.; Wong, W. Y. *Chem.—Eur. J.* **2012**, *18*, 1502.
(24) Wong, W. Y.; Ho, C. L. *Acc. Chem. Res.* **2010**, *43*, 1246.
(25) Emmert, L. A.; Choi, W.; Marshall, J. A.; Yang, J.; Meyer, L. A.; Brozik, J. A. *J. Phys. Chem. A* **2003**, *107*, 11340.
(26) Glik, E. A.; Kinayyigit, S.; Ronayne, K. L.; Towrie, M.; Sazanovich, I. V.; Weinstein, J. A.; Castellano, F. N. *Inorg. Chem.* **2008**, *47*, 6974.
(27) Cho, S.; Mara, M. W.; Wang, X. H.; Lockard, J. V.; Rachford, A. A.; Castellano, F. N.; Chen, L. X. *J. Phys. Chem. A* **2011**, *115*, 3990.
(28) Flynn, D. C.; Ramakrishna, G.; Yang, H. B.; Northrop, B. H.; Stang, P. J.; Goodson, T. *J. Am. Chem. Soc.* **2010**, *132*, 1348.
(29) Bhaskar, A.; Guda, R.; Haley, M. M.; Goodson, T., III. *J. Am. Chem. Soc.* **2006**, *128*, 13972.
(30) Wang, X.; Goeb, S.; Ji, Z.; Castellano, F. N. *J. Phys. Chem. B* **2010**, *114*, 14440.
(31) Zhao, G. J.; Yu, F. B; Zhang, M. X.; Northrop, B. H.; Yang, H. B; Han, K. L.; Stang, P. J. *J. Phys. Chem. A* **2011**, *115*, 6390.
(32) Zhao, G. J.; Northrop, B. H.; Stang, P. J.; Han, K. L. *J. Phys. Chem. A* **2010**, *114*, 3418.
(33) Zhao, G. J.; Northrop, B. H.; Han, K. L.; Stang, P. J. *J. Phys. Chem. A* **2010**, *114*, 9007.
(34) Zhao, G. J.; Han, K. L.; Stang, P. J. *J. Chem. Theory Comput.* **2009**, *5*, 1955.
(35) Chen, J. S.; Zhao, G. J.; Cook, T. R.; Sun, X. F.; Yang, S. Q.; Zhang, M. X.; Han, K. L.; Stang, P. J. *J. Phys. Chem. A* **2012**, *116*, 9911.
(36) Singh-Rachford, T. N.; Castellano, F. N. *J. Phys. Chem. Lett.* **2010**, *1*, 195.
(37) Lindgren, M.; Minaev, B.; Glimsdal, E.; Vestberg, R.; Westlund, R.; Malmstrom, E. *J. Lumin.* **2007**, *124*, 302.
(38) Grunder, S.; Huber, R.; Horhoiu, V.; Gonzalez, M. T.; Schonenberger, C.; Calame, M.; Mayor, M. *J. Org. Chem.* **2007**, *72*, 8337.
(39) Furche, F.; Ahlrichs, R. *J. Chem. Phys.* **2002**, *117*, 7433.
(40) Grimme, S.; Furche, F.; Ahlrichs, R. *Chem. Phys. Lett.* **2002**, *361*, 321.
(41) Schafer, A.; Huber, C.; Ahlrichs, R. *J. Chem. Phys.* **1994**, *100*, 5829.
(42) Ahlrichs, R.; Bar, M.; Haser, M.; Horn, H.; Kolmel, C. *Chem. Phys. Lett.* **1989**, *162*, 165.
(43) Von Arnim, M.; Ahlrichs, R. *J. Comput. Chem.* **1998**, *19*, 1746.
(44) Treutler, O.; Ahlrichs, R. *J. Chem. Phys.* **1995**, *102*, 346.
(45) Sierka, M.; Hogekamp, A.; Ahlrichs, R. *J. Chem. Phys.* **2003**, *118*, 9136.
(46) Eichkorn, K.; Treutler, O.; Ohm, H.; Haser, M.; Ahlrichs, R. *Chem. Phys. Lett.* **1995**, *242*, 652.
(47) Yanai, T. *Chem. Phys. Lett.* **2004**, *393*, 51.
(48) Botek, E.; d'Antuono, P.; Jacques, A.; Carion, R.; Champagne, B.; Maton, L.; Taziaux, D.; Habib-Jiwan, J. L. *Phys. Chem. Chem. Phys.* **2010**, *12*, 14172.
(49) Frisch, M. J.; Trucks, G. W.; Schlegel, H. B.; Scuseria, G. E.; Robb, M. A.; Cheeseman, J. R.; Scalmani, G.; Barone, V.; Mennucci, B.; Petersson, G. A.; Nakatsuji, H.; Caricato, M.; Li, X.; Hratchian, H. P.; Izmaylov, A. F.; Bloino, J.; Zheng, G.; Sonnenberg, J. L.; Hada, M.; Ehara, M.; Toyota, K.; Fukuda, R.; Hasegawa, J.; Ishida, M.; Nakajima, T.; Honda, Y.; Kitao, O.; Nakai, H.; Vreven, T.; Montgomery, J. A.; Jr.; Peralta, J. E.; Ogliaro, F.; Bearpark, M.; Heyd, J. J.; Brothers, E.; Kudin, K. N.; Staroverov, V. N.; Keith, T.; Kobayashi, R.; Normand, J.; Raghavachari, K.; Rendell, A.; Burant, J. C.; Iyengar, S. S.; Tomasi, J.; Cossi, M.; Rega, N.; Millam, J. M.; Klene, M.; Knox, J. E.; Cross, J. B.; Bakken, V.; Adamo, C.; Jaramillo, J.; Gomperts, R.; Stratmann, R. E.; Yazyev, O.; Austin, A. J.; Cammi, R.; Pomelli, C.; Ochterski, J. W.; Martin, R. L.; Morokuma, K.; Zakrzewski, V. G.; Voth, G. A.; Salvador, P.; Dannenberg, J. J.; Dapprich, S.; Daniels, A. D.; Farkas, O.; Foresman, J. B.; Ortiz, J. V.; Cioslowski, J.; Fox, D. J. *Gaussian 09*; Gaussian, Inc.: Wallingford, CT, 2010.
(50) Schafer, A.; Horn, H.; Ahlrichs, R. *J. Chem. Phys.* **1992**, *97*, 2571.
(51) Dawson, W. R.; Windsor, M. W. *J. Phys. Chem.* **1968**, *72*, 3251.
(52) *Modern Molecular Chemistry*; Turro, N. J., Ed.; University Science Books: Sausalito, CA, 1991; pp 146−148.
(53) Pomestchenko, I. E.; Castellano, F. N. *J. Phys. Chem. A* **2004**, *108*, 3485.

NOTE ADDED AFTER ASAP PUBLICATION

The caption of Figure 6 was incorrect in the version published ASAP on April 22, 2013. The corrected version was re-posted on May 1, 2013.